Journal of Luminescence 132 (2012) 345–349

Contents lists available at SciVerse ScienceDirect

Journal of Luminescence

journal homepage: www.elsevier.com/locate/jlumin

Photoluminescence study of polycrystalline $CsSnI_3$ thin films: Determination of exciton binding energy

Zhuo Chen [a,b], Chonglong Yu [a,b], Kai Shum [a,b,*], Jian J. Wang [c], William Pfenninger [c], Nemanja Vockic [c], John Midgley [c], John T. Kenney [c]

[a] Department of Physics, Brooklyn College of CUNY, Brooklyn, NY 11210, United States
[b] The Graduate Center of CUNY, 365 5th Avenue, New York, NY 10016, United States
[c] OmniPV Inc., 1030 Hamilton Court, Menlo Park, CA 94025, United States

ARTICLE INFO

Article history:
Received 13 May 2011
Received in revised form
12 July 2011
Accepted 2 September 2011
Available online 10 September 2011

Keywords:
Exciton
Radiative emission
Perovskite semiconductor
Photoluminescence

ABSTRACT

We report on the determination of exciton binding energy in perovskite semiconductor $CsSnI_3$ through a series of steady state and time-resolved photoluminescence measurements in a temperature range of 10–300 K. A large binding energy of 18 meV was deduced for this compound having a direct band gap of 1.32 eV at room temperature. We argue that the observed large binding energy is attributable to the exciton motion in the natural two-dimensional layers of SnI_4 tetragons in this material.

1. Introduction

Wannier [1] excitons provide many desirable optical properties of semiconductors such as enhanced spontaneous emission efficiency over free electron–hole recombination [2], low current thresholds for exciton or exciton-polariton lasers [3–5], and fast and large electro-absorption change in electro-optic modulators [6,7]. Large exciton binding energy is required to operate many exciton-related devices at room temperature because of the thermal dissociation of excitons to separated electrons and holes. Exciton binding energy is an intrinsic property for a given bulk semiconductor; it is known to obey the empirical energy band gap scaling law, i.e., proportional to its energy band gap [8,9]. Relatively low band gap semiconductors such as GaAs, CdSe, and their alloys have small exciton binding energies compared to the thermal energy of 26 meV at room temperature. Spatial exciton confinement either in one dimension, two dimensions, or three dimensions increases the binding energy of excitons and is nowadays widely used to produce many optoelectronic devices used in optical communication and light display.

There are many methods used to determine exciton binding energies depending on different material systems. For example, the exciton binding energy of 4.2 meV for bulk GaAs was accurately determined by the low temperature absorption measurements in which 1s and 2s excitonic absorption peaks were identified [10]. For polycrystalline semiconductor materials, inhomogeneous spectral line broadenings are usually large; it is difficult to determine exciton binding energy from the spectral information contained in photoluminescence, absorption, photocurrent, modulated-reflection, or photoexcitation spectra.

In this paper, we report on a specific method to determine the exciton binding energy in a polycrystalline $CsSnI_3$ compound using a set of temperature dependent photoluminescence (PL) data. A simple rate equation associated with the exciton generation, annihilation, and dissociation processes was used to interpret the temperature dependence of integrated steady state PL intensity using an exciton binding energy as a parameter to fit the data. A large exciton binding energy of 18 meV was deduced. We then verified the assumption used in the rate equation that the depopulation of photogenerated excitons was dominated only by the thermal dissociation and radiative spontaneous emission processes using time-resolved PL data. Furthermore, we argue that this large exciton binding energy is attributable to the exciton motion in natural two-dimensional (2D) arrays of SnI_4 tetragons. This argument is supported by the analytical expression of the total number of 2D excitons, which consistently explains the slow decreasing rate of the integrated steady-state PL intensity as a function of temperature. Finally, the 2D exciton model is tested using the normally accepted energy-gap scaling rule for exciton binding energy.

* Corresponding author at: Tel.: +1 718 951 5000.
E-mail address: kshum@brooklyn.cuny.edu (K. Shum).

0022-2313/$ - see front matter © 2011 Elsevier B.V. All rights reserved.
doi:10.1016/j.jlumin.2011.09.006

2. $CsSnI_3$ thin-film and PL experiment apparatus

Polycrystalline $CsSnI_3$ thin films, synthesized by vacuum evaporation of CsI and SnI_2 followed by a brief annealing to form $CsSnI_3$, were characterized [11] by surface and cross-section scanning electron microscopy (SEM) and transmission electron microscopy (TEM). A cross-sectional SEM image taken from a $CsSnI_3$ film on a ceramic substrate is shown in Fig. 1(a). The film is filled with polycrystalline domains with a typical size of $\sim$300 nm. TEM images were taken from several selected areas, showing different lattice spacing due to different crystal orientations. Electron diffraction patterns in these areas are typical ring-like patterns consistent with the nature of polycrystalline thin films. As discussed in the previous report [11], the crystal structure was verified by the X-ray diffraction data and by a close agreement between measured electron diffraction data and theoretical results calculated using the CASTEP simulation tool [12]. Fig. 1(b) displays a high resolution TEM image of a two-dimensional array of SnI_6 octahedra with a period of 4.2 ± 0.1 Å. This octahedra array matches with the theoretically generated counterpart with a period of 4.3 Å as displayed in Fig. 1(c). It has also been determined [11] that $CsSnI_3$ compound is a direct band gap semiconductor having a band gap of 1.32 eV at room temperature.

PL spectra were taken from a nanolog system from Horiba Jobin Yvon. It consists of a light source (450 W Xe lamp), a double-grating excitation spectrometer to select a central excitation wavelength and its bandwidth, a sample compartment either fiber-coupled or in free-space optics to collect PL, and an emission spectrometer to spectrally select desired emission to a photomultiplier tube (PMT), coupled with time-correlated single photon counting electronic circuits. For the PL in a spectral range of 800–1050 nm, a Hamamatsu PMT tube (P2658P) was used. Another Hamamatsu PMT tube (H10330-75) was used for searching the impurity-related PL in the spectral range of 1050–1500 nm. Photoexcitation level was low and was about 20 mW/cm^2 for steady state PL measurements. For temperature dependent PL measurements, a sample was attached to the cold finger of a cryostat system capable of varying the temperature from 4 to 350 K. A picosecond laser from High-Q-Laser was used for time-resolved and photoexcitation-dependent PL measurements as an excitation source producing 532 nm optical pulses of 8 ps at a repetition rate of 76 MHz. The overall time resolution is about 200 ps for this system, mainly limited by the PMT used.

3. Photoluminescence data and discussions

Fig. 2(a) displays the temperature dependent PL spectra from one of the best $CsSnI_3$ thin-film samples. It shows the decrease of PL peak intensity and the spectral line broadening with increasing temperature from 10 to 300 K. The integrated PL over the full spectrum decreases with temperature as shown in Fig. 2(b). It should be pointed out here that the PL peak position monotonically shifts to higher energy as temperature increases, a different behavior as compared to most of the semiconductors. This implies the energy band gap increases as temperature increases. The

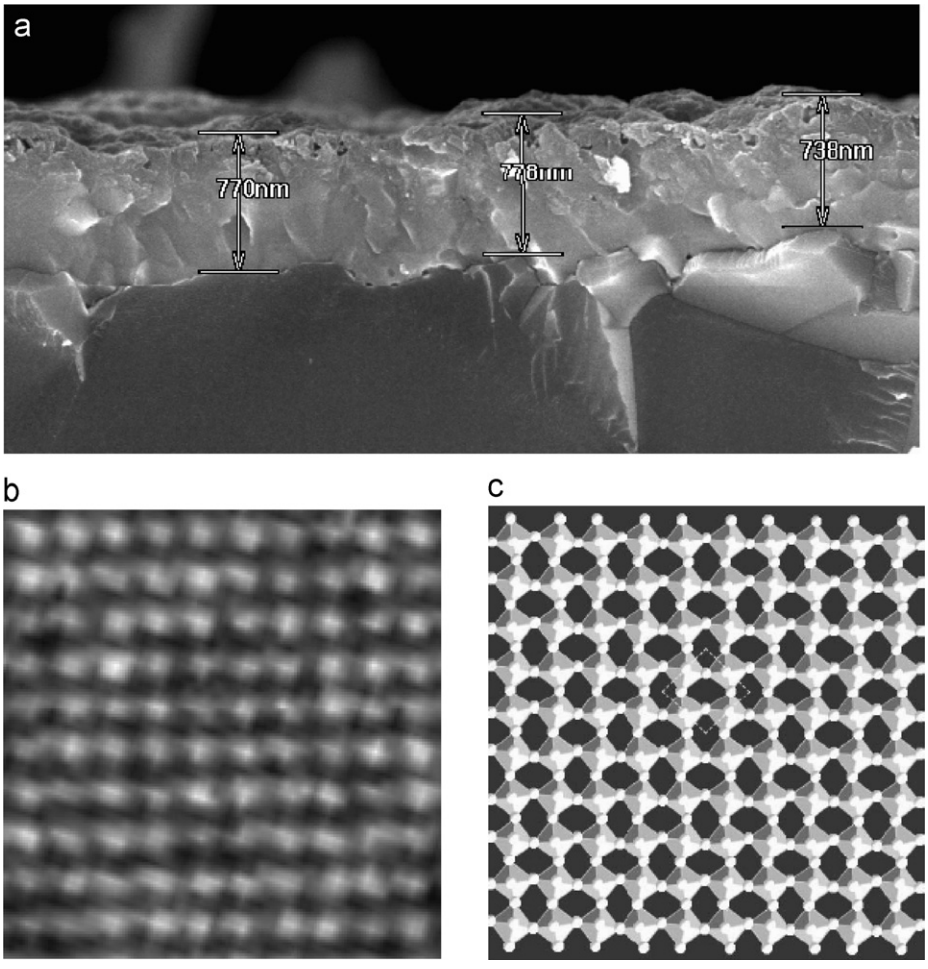

Fig. 1. (a) Cross-sectional SEM for a $CsSnI_3$ film on a ceramic substrate. (b) High resolution TEM in a selected area. (c) Theoretically generated 10×10 octahedra with tin atoms at the centers and iodine atoms at vertices, projected into an ***xy*** plane with ***x***=[−1 1 0] and ***y***=[1 1 0].

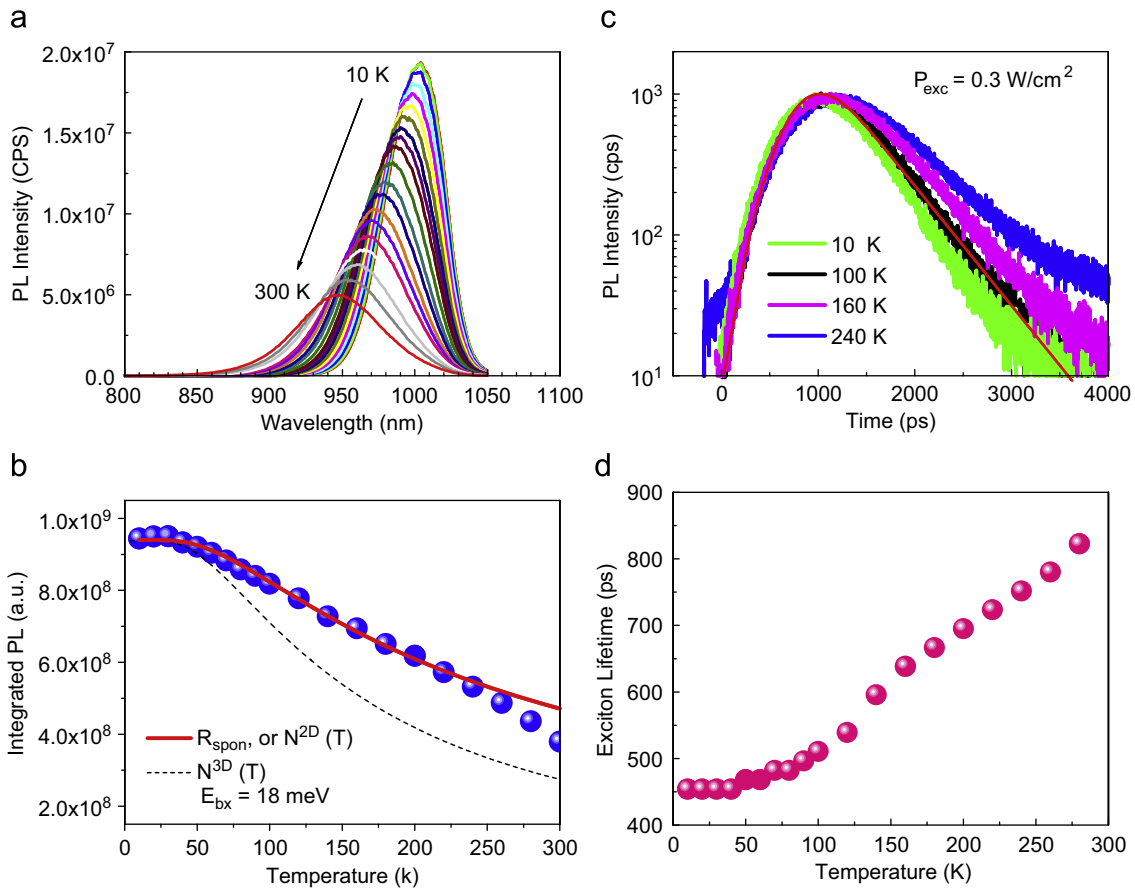

Fig. 2. (a) PL spectra from 10 to 300 K for one of the best samples we studied, excited by a Xe-lamp with the excitation power density of ~20 mW/cm^2 at 500 nm with a 5 nm bandwidth. (b) Integrated PL intensity from spectra shown in (a) as a function of temperature. The red (solid) curve is calculated with the exciton binding energy of 18 meV using either Eq. (2) or Eq. (3). The dashed curve plots the total number of excitons as a function of temperature using the three-dimensional DOS. (c) Time-resolved PL profiles at the emission peak at various temperatures. A thin (smooth) red curve shows a convolution fit at $T=100$ K by the Gaussian system response function and a single PL decay time of 515 ps. (d) Measured exciton lifetime is plotted as spheres at various temperatures (for interpretation of the references to color in this figure legend, the reader is referred to the web version of this article).

detailed discussion of this behavior will be presented elsewhere. We will focus on the discussion of the decrease of integrated PL as temperature increases. Apparently, it is common for the integrated PL to decrease with increasing temperature, simply because non-radiative channels may become active as temperature increases. What is unique for this compound and is also pivotal to simply determine the exciton binding energy in this compound is the rate of PL decreasing. This rate is much slower than that of most common direct band gap semiconductors such as InGaAs and GaAs epitaxial layers even grown on lattice-matched crystalline substrates in a large temperature range of 10–300 K. As quantitatively analyzed below, the slow PL decrease rate arises from the fact that in this compound, the thermal ionization of excitons is only comparable to non-radiative process that competes with radiative exciton annihilation process.

When we assume that the measured PL arises from excitonic annihilations and the decrease in PL intensity is only due to the increase in thermal dissociation rate of excitons at higher temperatures, then the following rate equation should hold:

$$R_G = R_{spon} + A\exp\left(-\frac{E_{bx}}{K_B T}\right). \quad (1)$$

where R_G is the exciton generation rate maintained by photoexcitation and R_{spon} is the spontaneous emission rate giving rise to PL; the last term in Eq. (1) is the thermal dissociation rate for excitons, with the exciton binding energy, E_{bx}, as the activation energy for ionization. With the limiting condition of $R_{spon} \to 0$ when $T \to \infty$, $A=R_G$, Eq. (1) becomes

$$R_{spon} = R_G\left[1-\exp\left(-\frac{E_{bx}}{K_B T}\right)\right]. \quad (2)$$

Since R_{spon} is proportional to the integrated PL intensity, by fitting Eq. (2) to the experimental data displayed in Fig. 2(b), the value of exciton binding energy, 18 meV, is determined based on this model. Before discussing this relatively large exciton binding energy value, it is necessary to provide an evidence to validate Eq. (1), i.e. to show the radiative exciton annihilation process dominates all non-radiative processes. Picosecond time-resolved PL technique is a direct and useful tool to deliver such a proof.

Time-resolved PL data were taken in a temperature range of 10–300 K from the same sample we took the steady state PL spectra. They are displayed in Fig. 2(c). Each PL decay curve was fitted by a convolution of the system response function with a single exponential decay constant, τ_d. The fit at 100 K, as an example, is shown as a thin red curve. The value of the PL decay constant, inversely proportional to the PL decay rate, is normally dictated by radiative and non-radiative processes, i.e., $\tau_d = \tau_r/(1+\tau_r/\tau_{nr})$, where τ_r and τ_{nr} are the respective decay constants for these two processes. The fact that decay constant, as shown in Fig. 2(d), monotonically increases with temperature demonstrates that radiative exciton decay is indeed the dominant process; hence, $\tau_d \sim \tau_r$. This key evidence clearly supports the assumption used in the rate equation (1).

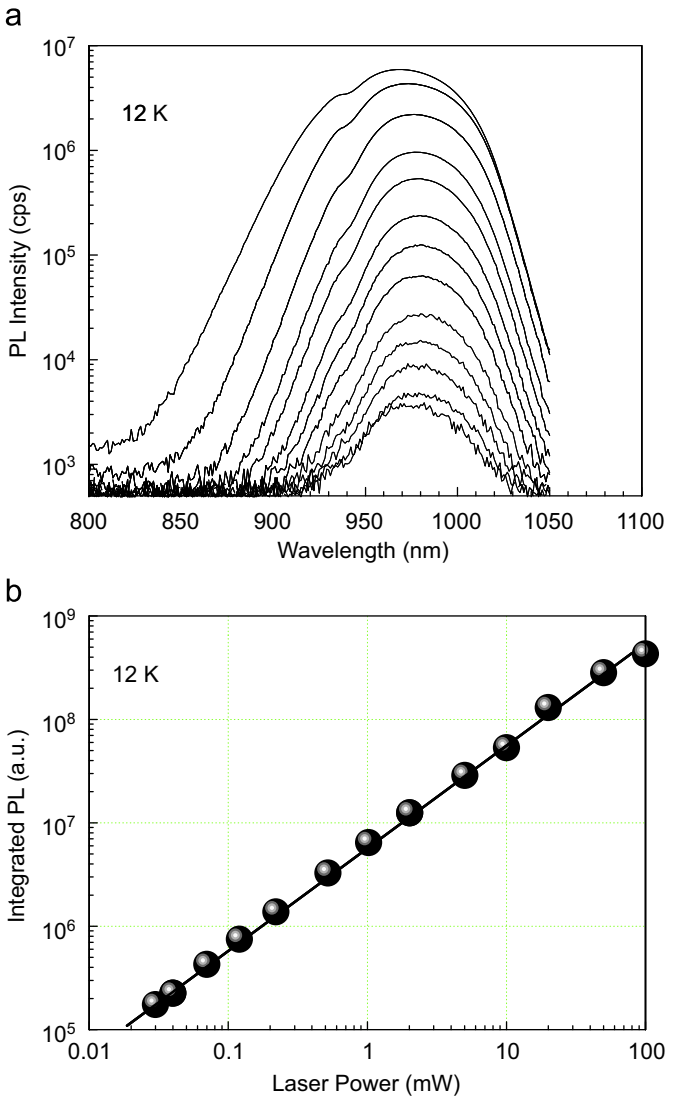

Fig. 3. (a) PL spectra at 12 K are displayed with laser excitation power from 0.03 to 100 mW. The maximum exciton density is estimated to be on the order of $10^{16}\,cm^{-3}$. Note the spectra are not spectrally corrected and small dip in the spectra at 945 nm is due to the fiber used to collect PL. (b) Integrated PL intensity shown in (a) vs. excitation laser power. The thin line indicates the PL linearity with laser excitation power.

A linear dependence of integrated PL intensity as a function of photoexcitation power at a given temperature is usually considered to be one of the necessary criteria for excitonic emissions. Fig. 3(a) displays the PL spectra as the laser excitation power increases from 0.03 to 100 mW at 12 K. For this experiment, PL was collected and delivered through an optical fiber bundle manufactured by Ocean Optics. The PL spectra were not spectrally corrected since we were only interested in the relative integrated PL intensity as a function of increasing photoexcitation power. The integrated PL intensity vs. excitation power is displayed in Fig. 3(b) showing near three orders of magnitude of the PL linearity over the excitation power. The thin solid line shows the gradient of one indicating constant PL efficiency over the four orders of magnitude change in photoexcitation power. This linear excitation power dependence further validates the exciton model manifested by Eq. (2).

Although the PL linearity on photoexcitation power over the four orders of magnitude without saturation up to the maximum exciton density of $\sim 10^{16}\,cm^{-3}$ suggests that the origin of PL is intrinsic rather than extrinsic, we provide more evidences next to confirm that the excitons in our exciton model are free excitons (FE), not a kind of bound excitons (BE) such as bound to neutral or ionized donors (acceptors) or even a combination of various types of bound excitons. A strong evidence of the FE assignment comes from the spectral shape of PL; it clearly shows a broad single peak with a high energy tail gradually developing as the sample temperature increases from 10 to 300 K. If the measured PL were from BE, we would expect a FE shoulder getting strength as the sample temperature increases while the relative strength of BE to FE decreases. This scenario of the temperature dependent PL from BE with an additional binding energy to impurities on an order of 20 meV has been observed for ZnO [13,14] and GaN [15,16]. The fact that we do not observe a shoulder on PL spectra is consistent with the intrinsic PL origin.

According to Hayne's rule [17] donor (acceptor) energy levels would be about 120–180 meV below (above) the conduction (valence) band edge if the deduced 18 meV were considered as an additional binding energy to these impurities. If there were a substantial amount of impurities, we would expect to observe one or more of the following impurity related optical transitions: (1) donor-electron to valence band hole, (2) conduction band electron to acceptor-hole, (3) donor electron to conduction band, and (4) valence band electron to acceptor hole. Since we did not measure any PL from 1050 to 1500 nm, the optical transition of (1) or (2) was not detectable. For the (3) or (4) transition, a Fourier transform infrared (FTIR) spectrometer was used to measure the impurity absorption features. As shown in Fig. 4, other than a weak absorption spike at 83 meV [18] and a doublet at 290/293 meV [18,19] displayed in the inset due to residual CO_2, there are no other absorption features in the energy range of 65–325 meV on the measured absorbance spectrum at room temperature, taking from a 400 nm $CsSnI_3$ thin-film deposited on a CsI substrate. The absence of any optical transitions of (1)–(4) demonstrates that the density of impurities (if there are) is below the FTIR impurity detection limit of 0.03 ppm [20], which is equivalent to an impurity density of $\sim 10^{15}\,cm^{-3}$ [21]. This demonstration is consistent with the high PL efficiency even up to room temperature and further confirms our FE assignment.

We now turn to the discussion on why the exciton binding energy in this semiconductor compound is much larger than expected [8,9] based on its value of energy band gap, 1.32 eV

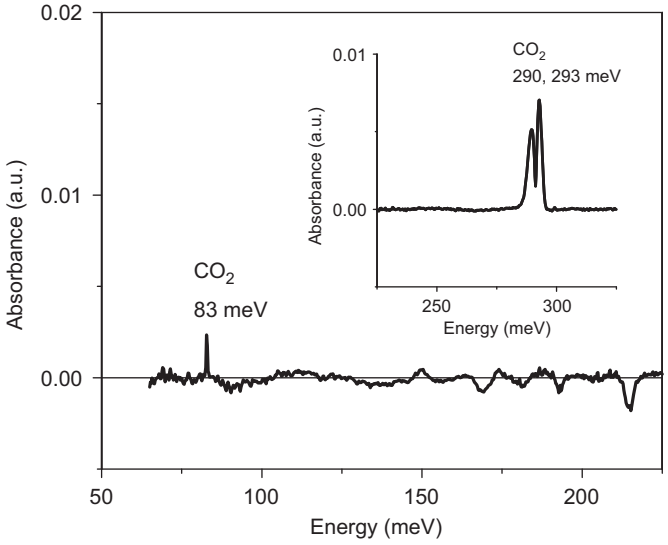

Fig. 4. FTIR absorbance spectrum of $CsSnI_3$ thin film on CsI substrate at room temperature. A spike at 83 meV and a doublet at 290/293 meV displayed in the inset are due to residual CO_2 gas in the sample compartment. No infrared optical transitions were measured due to impurity states within the $CsSnI_3$ energy gap.

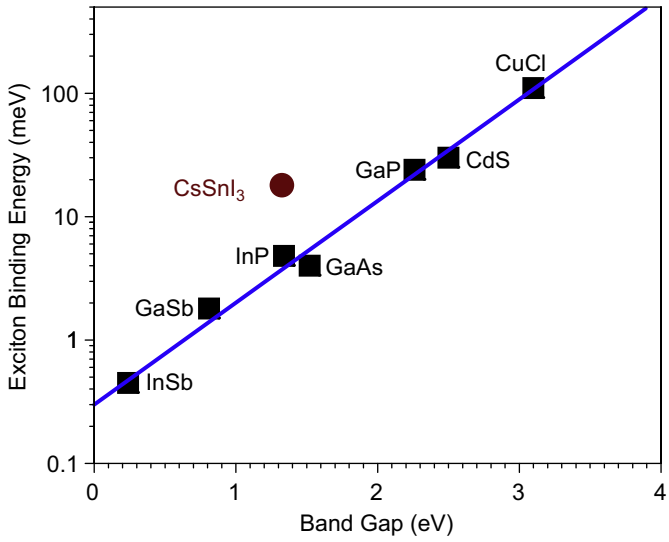

Fig. 5. Exciton binding energies in various semiconductors (filled squares) are plotted as their host semiconductor band gap energy, E_g. The exciton binding energy in $CsSnI_3$ is indicated as a filled circle. The linear line is calculated by the expression $E_{bx}(\text{meV}) = 0.3e^{1.9E_g(\text{eV})}$.

at 300 K. As shown in Fig. 5, the data point of 18 meV for $CsSnI_3$ as a filled circle appears to be an outlier. We start with the assumption that the photogenerated excitons in this material are two-dimensional (2D) excitons residing in the 2D layers of SnI_4 tetragons as suggested by the high resolution TEM image shown in Fig. 1(b). There are two verifiable outcomes based on this assumption. First, the energy independent 2D excitonic density of states (DOS) is distinctly different from the energy dependent DOS for one-dimensional or two-dimensional exciton motion. Using the 2D DOS and the Boltzmann distribution, the total number of excitons at a given temperature is given by

$$N^{2D}(T) = N_0\left[1-\exp\left(-\frac{E_{bx}}{K_B T}\right)\right], \quad (3)$$

where N_0 is the number of total excitons at 0 K. The temperature dependent integrated PL should be proportional to the total number of excitons that can be maintained in the film at a given temperature. Therefore, Eq. (3) can also be used to fit the data in Fig. 2(b). As it is obvious just from the form of Eq. (3), the fit to the experimental data should be excellent, which supports the 2D exciton assumption. We also calculated the total exciton number as a function of temperature using the three-dimensional DOS to fit the data as shown in Fig. 2(b) by dashed curve. It clearly fails to fit the data. Second, if the assumption is correct, a three-dimensional exciton binding energy for this compound would be one fourth of 18 meV, i.e., 4.5 meV. This number is consistent to the band energy gap scaling law for exciton binding energy, which is plotted as a solid line in Fig. 5. Although there were reports on natural 2D excitons in PbI_4- [22,23] and $PbCl_4$-based [24] inorganic–organic hybrid materials, the physical reasons why the excitons in this material prefer 2D motion awaits further investigations.

4. Conclusions

In conclusion, we have experimentally determined the value of exciton binding energy in $CsSnI_3$, a perovskite semiconductor compound, using a series of photoluminescence measurements. The fact that the deduced exciton binding energy, 18 meV, is much larger than expected based on the empirical band gap energy scaling law strongly suggests the motion of non-resonantly photoexcited excitons in $CsSnI_3$ is two-dimensional in the 2D layers of SnI_4 tetragons. This method of exciton binging energy determination is applicable to other materials only when the depopulation of photogenerated excitons is dominated by the thermal dissociation and radiative spontaneous emission processes.

Acknowledgments

This work at Brooklyn College was partially supported by OmniPV Corporation and by New York State Foundation for Science, Technology, and Innovation (NYSTAR) through the Photonics Center of the City University of New York.

References

[1] G.H. Wannier, Phys. Rev. 52 (1937) 191.
[2] G.W. Hooft, W.A.J.A. Van der Poel, L.W. Molen, C.T. Foxon, Phys. Rev. B 35 (1987) 8281.
[3] H. Deng, C. Weihs, D. Snoke, J. Block, Y. Yamamato, PNAS 100 (2003) 15318.
[4] S. Christopoulos, G. Baldassarri, H. von Hoersthal, A.J.D. Gundy, P.G. Lagondakis, A.V. Kavokin, J.J. Baumberg, G. Christman, R. Rutle, E. feltin, J.–F. Carlin, N. Grandjean, Phys. Rev. Lett. 98 (2007) 126405.
[5] Sheng Chu, M. olmedo, Z. Yang, J. Kong, J. Liu, Appl. Phys. Lett. 93 (2008) 181106.
[6] D.A.B. Miller, D.S. Chemla, T.C. Damen, A.C. Gossard, W. Wiegmann, T.H. Wood, C.A. Burrus, Phys. Rev. Lett. 53 (1984) 2173.
[7] E.A. De Soza, L. Carraresi, G.D. Boyd, D.A.B. Miller, Opt. Lett 18 (1993) 974.
[8] H. Haug, S.W. Koch, Quantum Theory of the Optical and Electronic Properties of Semiconductor, World Scientific, 1990 (p.164).
[9] D.C. Reynolds, T.C. Collins, Excitons, their Properties and Uses, Academic Press, 1981 (p. 270).
[10] D.D. Sell, Phys. Rev. B 6 (1972) 3750.
[11] Kai Shum, Z. Chen, J. Qureshi, C. Yu, J.J. Wang, W. Pfenninger, N. Vockic, J. Midgley, J.T. Kenney, Appl. Phys. Lett. 96 (2010) 221903.
[12] 〈http://accelrys.com/products/materials-studio/modules/CASTEP.html〉.
[13] D.W. Hamby, D.A. Lucca, M.J. Klopfstein, G. Cantwell, J. Appl. Phys. 93 (2003) 3214.
[14] P. Misra, T.K. Sharma, L.M. Kukreja, Curr. Appl. Phys. 9 (2009) 179.
[15] W. Shan, X.C. Xie, J.J. Song, B. Goldenburg, Appl. Phys. Lett. 67 (1995) 2512.
[16] L. Eckey, et al., Appl. Phys. Lett. 68 (1996) 415.
[17] J.R. Haynes, Phys. Rev. Lett. 4 (1960) 361.
[18] C.–P. Sherman Hsu, in: F.A. Settle (Ed.), Instrumental Techniques for Analytical Chemistry, Prentice Hall, 1997, p. 257.
[19] T. Schweizer, D.W. Hewak, B.N. Samson, D.N. Payne, Opt. Lett. 21 (1996) 1594.
[20] R.R. Mattews, L.A. Melton, Anal. Chem. 58 (1986) 807.
[21] W.J. Moore, et al., Appl. Phys. Lett. 79 (2001) 2570.
[22] T. Kenichiro Tanaka, I. Takahashi, T. Kondo, K. Umebajashi, Asai, K. Ema, Phys. Rev. B 71 (2005) 045312.
[23] G. Lanty, J.S. Lauret, E. Deleporte, S. Bouchoule, X. Lafosse, Appl. Phys. Lett. 93 (2008) 081101.
[24] G. Sanjun Zhang, J.–S. Lanty, E. Lauret, P. Deleporte, Audbert, L. Galmiche, Acta Mater. 57 (2009) 3301.